International Journal of Impact Engineering 36 (2009) 1116–1127

Contents lists available at ScienceDirect

International Journal of Impact Engineering

journal homepage: www.elsevier.com/locate/ijimpeng

Using split Hopkinson pressure bars to perform large strain compression tests on polyurea at low, intermediate and high strain rates

Jongmin Shim [a], Dirk Mohr [a,b,*]

[a] Impact and Crashworthiness Laboratory, Department of Mechanical Engineering, Massachusetts Institute of Technology, Cambridge, MA 02139, USA
[b] Solid Mechanics Laboratory (CNRS-UMR 7649), Department of Mechanics, École Polytechnique, Palaiseau, France

ARTICLE INFO

Article history:
Received 23 September 2008
Received in revised form
12 December 2008
Accepted 16 December 2008
Available online 25 December 2008

Keywords:
Split Hopkinson pressure bar
Wave deconvolution
Polyurea
Intermediate strain rates

ABSTRACT

The strain rate sensitivity of polyurea is characterized using a modified split Hopkinson pressure bar (SHPB) system. The device is composed of a hydraulic piston along with nylon input and output bars. In combination with an advanced wave deconvolution method, the modified SHPB system provides an unlimited measurement time and thus can be used to perform experiments at low, intermediate and high strain rates. A series of compression tests of polyurea is performed using the modified SHPB system. In addition, conventional SHPB systems as well as a universal hydraulic testing machine are employed to confirm the validity of the modified SHBP technique at low and high strain rates. The analysis of the data at intermediate strain rates shows that the strain rate is not constant due to multiple wave reflections within the input and output bars. It is demonstrated that intermediate strain rate SHPB experiments require either very long bars (>20 m) or very short bars (<0.5 m) in order to achieve an approximately constant strain rate throughout the entire experiment.

1. Introduction

Polyurea is a special type of elastomer which is widely used as coating material. It features a fast setting time (few minutes or less) as well as good chemical and fire resistance. Polyurea is frequently used on metallic substrates where it provides corrosion and abrasion resistance in harsh environments. Applications include transportation vehicles, pipelines, steel buildings or marine constructions. More recently, polyurea is also considered for the blast protection of transportation vehicles because of its high toughness-to-density ratio, in particular at high strain rates. It is the objective of this work to characterize the mechanical properties polyurea at low, intermediate and high strain rates.

The mechanical properties of most metallic engineering materials exhibit only a weak rate-dependence at strain rates below 100/s. Therefore, metals are usually tested either at very low strain rates ($<10^{-2}$/s) on universal testing machines or at high strain rates (10^{2}/s) on split Hopkinson pressure bar (SHPB) systems. The stress–strain response of most polymeric materials on the other hand shows a pronounced strain rate sensitivity at low, intermediate and high strain rates. At small strains, the viscoelastic properties of polymers are typically determined using dynamic mechanical analysis (e.g. McGrum et al. [1]). The characterization of the large deformation response of polymers at low and intermediate strain rates of up to 10/s can be performed on hydraulic testing systems (e.g. Yi et al. [2], Song et al. [3]). As for metals, conventional SHPB systems are employed to characterize the large deformation response of polymeric materials at high strain rates. However, as discussed by Gray and Blumenthal [4], low impedance Hopkinson bars are recommended when testing soft polymeric materials (e.g. Zhao et al. [5], Chen et al. [6], Sharma et al. [7]). Hoo Fatt and Bekar [8] developed a pulley system to perform large strain tensile tests on rubber sheets at intermediate and high strain rates. Inspired by this work, Roland et al. [9] designed a pendulum impact tester to study the tensile properties of elastomers at strain rates of up to about 500/s. In both testing systems, the issues related to the strain measurements under dynamic loading conditions are circumvented through the use of digital image correlation (DIC) based on high speed camera recordings.

Unlike for high strain rate experiments, the duration of the experiment poses a major challenge when using SHPB systems for intermediate strain rate testing. The experiment duration T_{exp} is given by the ratio of the strain ε_{max} at the end of the experiment and the average strain rate $\dot{\varepsilon}$, $T_{exp} = \varepsilon_{max}/\dot{\varepsilon}$. In order to avoid the superposition of waves, the maximum duration of reliable

* Corresponding author. Impact and Crashworthiness Laboratory, Department of Mechanical Engineering, Massachusetts Institute of Technology, Room 5-222, 77 Massachusetts Avenue, Cambridge, MA 02139, USA.
E-mail address: mohr@mit.edu (D. Mohr).

0734-743X/$ – see front matter © 2009 Elsevier Ltd. All rights reserved.
doi:10.1016/j.ijimpeng.2008.12.010

measurements is limited to the input bar transit time. The input bar transit time is an intrinsic property of the input bar and can only be lengthened by increasing the bar length or by choosing a bar material of low wave propagation speed. In combination with two strain measurements on each Hopkinson bar, wave separation techniques may be used to overcome this limitation for elastic (e.g. Lundberg and Henchoz [10], Yanagihara [11], Park and Zhou [12]) and viscoelastic bar systems (e.g. Zhao and Gary [13], Bacon [14], Casem et al. [15]). However, Jacquelin and Hamelin [16,17] as well as Bussac et al. [18] have shown that so-called two-point measurement wave separation techniques are sensitive to noise. This finding led to the development of a mathematical framework for an advanced wave deconvolution technique which is based on redundant measurements (Bussac et al. [18]). Othman and Gary [19] demonstrated the applicability of this testing technique to the intermediate strain rate testing of aluminum on a hydraulic actuator driven SHPB system. Othman et al. [20] also employed this technique when using a 0.82 m long bar to measure the axial forces in a modified servo-hydraulic machine. In the present work, we make use of a similar testing system as Othman and Gary [19] to characterize the intermediate strain rate response of the elastomeric material polyurea under compressive loading.

Various authors published experimental results on the strain rate sensitive response of amorphous glassy polymers (e.g. Chou et al. [21], Boyce et al. [22], Walley et al. [23], Cady et al. [24], Siviour et al. [25], Mulliken and Boyce [26], Mulliken et al. [27]), crystalline glassy polymers (e.g. Chou et al. [21], Bordonaro and Krempl [28], Cady et al. [24], Siviour et al. [25], Khan and Farrokh [29]) and elastomers (e.g. Gray et al. [30], Rao et al. [31], Song and Chen [32,33], Hoo Fatt and Bekar [8], Shergold et al. [34], Roland [35]) including polyurea (e.g. Amirkhizi et al. [36], Roland et al. [9], Sarva et al. [37]). However, only few experimental studies deal with the intermediate strain rate behavior of elastomers at large deformations. Sarva et al. [37] performed intermediate strain rate compression tests on polyurea for maximum strains greater than 100%, but the strain rates were only 14–80/s. The same research group also obtained test results for a strain rate of 800/s using a very long aluminum SHPB system. Roland et al. [9] characterized the tensile behavior of polyurea over a strain rate range of 14–573/s and up to strains of more than 300%. In the present study, an attempt is made to cover a similar range of strain rates by using the modified SHPB system of Zhao and Gary [13] in combination with the deconvolution method of Bussac et al. [18] to perform compression experiments on polyurea.

This paper is organized as follows. Section 2 describes all experimental procedures, notably the modified SHPB systems. The experimental results on polyurea are presented in Section 3, followed by a discussion of the limitations of the present testing system in Section 4.

2. Experimental procedures

Three different testing systems are used to cover a wide range of strain rates: a universal testing machine, a conventional SHPB system, and a modified SHPB system with a hydraulic actuator. Throughout our presentation of the experimental methods, we use the hat symbol to denote the Fourier transforms $\widehat{f}(\omega) = \int_{-\infty}^{\infty} f(t)e^{-i\omega t}\mathrm{d}t$ of time-dependent functions $f(t)$.

2.1. Universal testing machine

A hydraulic universal testing machine (Model 8800, Instron, Canton, MA) is used to perform compression tests at low and intermediate strain rates (10^{-2}–10/s). The position of the vertical actuator is controlled using the software MAX (Instron, Canton). The axial force $F(t)$ is measured using a low profile load cell of a maximum loading capacity of 10 kN (MTS, Chicago, IL) that has been positioned at a distance of 25 mm from the specimen. At the same time, the cross-head displacement is measured using an LVDT positioned at a distance of about 1300 mm above the specimen (integrated in the actuator piston). A DIC system (Vic2D, Correlated Solutions, Columbia, SC) is employed to measure the displacements $u_{\mathrm{in}}(t)$ and $u_{\mathrm{out}}(t)$ of the top and bottom loading platens, respectively. Furthermore, we make use of the DIC system to quantify the Poisson's ratio of polyurea. Both a thin polymer layer (Teflon) and grease are used to minimize the frictional forces at the contact surface between the specimen and the loading platens.

2.2. Conventional SHPB systems

Two distinct conventional SHPB systems are used in this study:

1) The first is an aluminum bar system with a 1203 mm long striker bar. Experiments of a maximum duration of $T_{\mathrm{exp}} = 472$ μs can be performed on this system.
2) The second SHPB system is composed of thermoplastic nylon bars with a 1092 mm long striker bar. Thus, a maximum duration of $T_{\mathrm{exp}} = 1255$ μs is achieved on that system.

Technical details of these systems are given in Table 1. The gages for strain history recordings are positioned near the center of the input bar and near the output bar/specimen interface (Table 1, Fig. 1a). Using viscoelastic wave propagation theory (e.g. Zhao and Gary [13]), we reconstruct the incident and reflected waves based on the input bar strain gage recordings to estimate the force $F_{\mathrm{in}}(t)$ and displacement $u_{\mathrm{in}}(t)$ at the input bar/specimen interface. Analogously, the force $F_{\mathrm{out}}(t)$ and displacement $u_{\mathrm{out}}(t)$ at the output bar/specimen interfaces are calculated after reconstructing the transmitted wave based on the output bar strain gage recording.

2.3. Modified SHPB with hydraulic actuator

The total duration of the loading pulse in an experiment on a conventional SHPB system is limited by the length of the striker bar. Thus, it is usually impossible to reach large strains at intermediate strain rates on conventional SHPB systems. To overcome this key limitation, we make use of the modified SHPB system proposed by Zhao and Gary [13]. By substituting the striker bar

Table 1
Specifications of the conventional SHPB systems.

	Aluminum bar system			Nylon bar system		
	striker	input bar	output bar	striker	input bar	output bar
Length, L [m]	1.203	2.991	1.850	1.092	3.070	1.919
Radius, R [mm]	20	20	20	16.5	20	20
Longitudinal wave speed, $c_0(\omega = 0)$ [m/s]	5100	5100	5100	1740	1740	1740
Mass density, ρ [kg/m^3]	2820	2820	2820	1187	1162	1145
Distance between strain gage and specimen/bar interface, d [m]	–	1.493	0.335	–	1.537	0.394

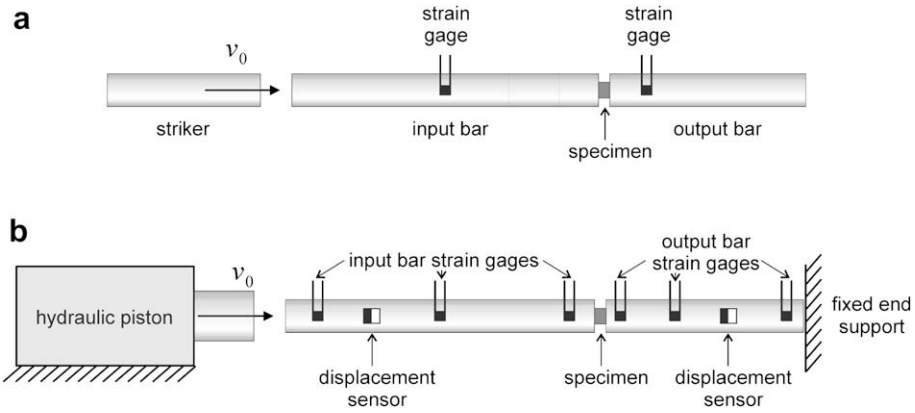

Fig. 1. (a) Conventional and (b) modified SHPB systems.

through a hydraulic actuator, almost infinite loading pulse durations may be achieved. Having this setting, the right end of the output bar needs to be fixed in space as its inertia is no longer sufficient to support the specimen (Fig. 1b). In order to prevent the failure of the nylon bars under excessive loads (it can be difficult to stop the piston), a fixed end support system is designed such that the bars are released before elastic buckling occurs. Note that the wave superposition in the input and output bars can no longer be avoided when the test duration T_{exp} exceeds the transit time for waves traveling from one bar end to the other. Therefore, a wave separation technique is employed to reconstruct the rightward and leftward traveling waves in the bars based on strain gage measurements. Once both the rightward and leftward traveling waves in the bars are known, the interface forces and velocities may be calculated using the same equations as those for the input bar in a conventional SHPB system. Wave separation techniques in the time domain are efficient for non-dispersive bars (e.g. Lundberg and Henchoz [10]), but these require more intense computations for waves in dispersive systems (e.g. Bacon [14]). Here, we adopt the frequency domain based deconvolution technique of Bussac et al. [18]. In particular, displacement measurements are included in addition to strain gage recordings.

Suppose that a strain wave $\varepsilon(x, t)$ in a bar is composed of the rightward traveling wave $\varepsilon_R(x, t)$ and the leftward traveling wave $\varepsilon_L(x, t)$. In terms of Fourier transforms, we have the multiplicative decomposition of the frequency and spatial dependence,

$$\widehat{\varepsilon}(x,\omega) = \widehat{\varepsilon}_R(x_0,\omega)e^{-i\xi(\omega)(x-x_0)} + \widehat{\varepsilon}_L(x_0,\omega)e^{i\xi(\omega)(x-x_0)} \tag{1}$$

where $\widehat{\varepsilon}_R(x_0,\omega)$ and $\widehat{\varepsilon}_L(x_0,\omega)$ denote the Fourier transform of the respective strain histories at some reference location x_0. $\xi(\omega)$ is the frequency-dependent wave propagation coefficient for the respective bar system,

$$\xi(\omega) = \kappa(\omega) + i\overline{\alpha}(\omega) = \frac{\omega}{c(\omega)} + i\overline{\alpha}(\omega), \tag{2}$$

with the frequency-dependent wave number $\kappa(\omega)$, the longitudinal wave propagation speed $c(\omega) = \omega/\kappa(\omega)$, and the attenuation coefficient $\overline{\alpha}(\omega)$.

The simplest approach to determine the functions $\widehat{\varepsilon}_R(x_0,\omega)$ and $\widehat{\varepsilon}_L(x_0,\omega)$ is to measure the strain histories $\varepsilon(x_1, t)$ and $\varepsilon(x_2, t)$ associated with the wave $\varepsilon(x, t)$ at two distinct locations x_1 and x_2 (on the same bar). Subsequently, one can solve the linear system of equations

$$\mathbf{b} = \mathbf{A}\mathbf{x} \tag{3}$$

with the unknowns

$$\mathbf{x}(\omega) = \begin{bmatrix} \widehat{\varepsilon}_R(x_0,\omega) \\ \widehat{\varepsilon}_L(x_0,\omega) \end{bmatrix}, \tag{4}$$

the measurements

Table 2
Specifications of the modified nylon SHPB system.

	input bar	output bar
Length, L [m]	3.123	3.045
Diameter, D [mm]	40	40
Longitudinal wave speed, $c_0(\omega = 0)$ [m/s]	1740	1740
Mass density, ρ [kg/m^3]	1150	1150
Distances between strain gages	0.61	0.825
and specimen/bar interface, d_{sg} [m]	1.515	1.523
	2.623	2.582
Distance between displacement sensor	0.953	2.183
and specimen/bar interface, d_{dm} [m]		

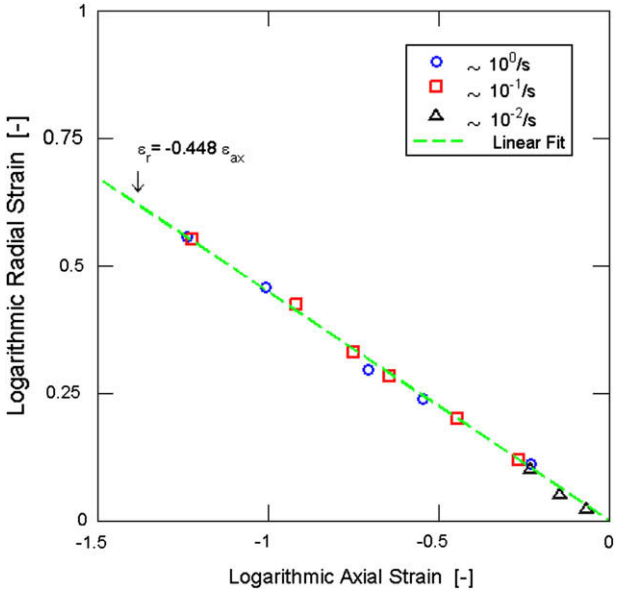

Fig. 2. Identification of Poisson's ratio from the linear relationship between the logarithmic radial and axial strains.

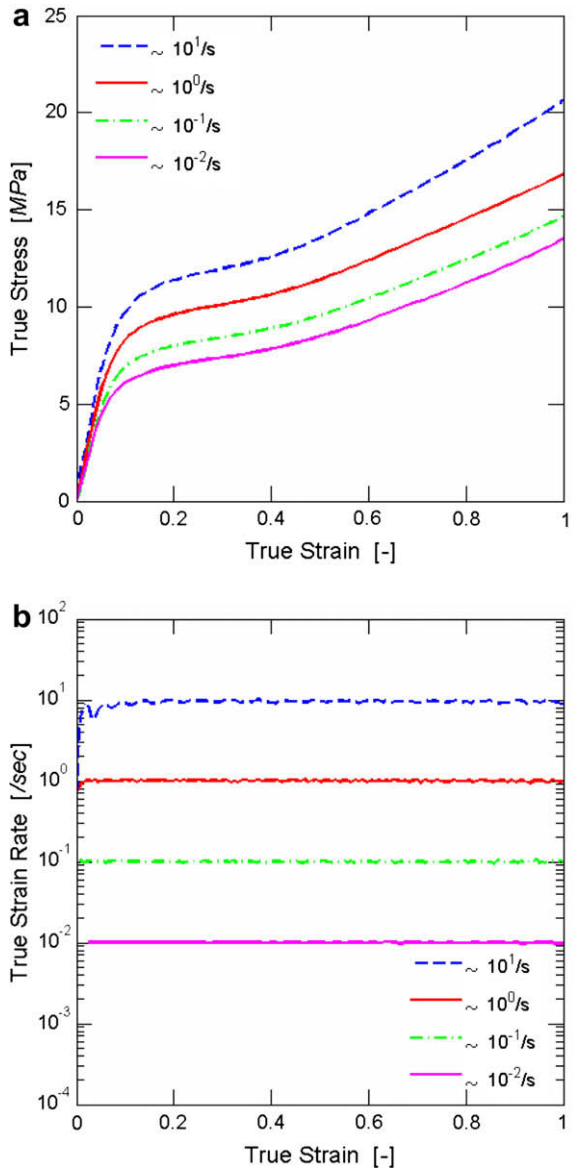

Fig. 3. Test results from the universal testing machine: (a) True stress–strain curves, (b) True strain versus true strain curves.

$$\mathbf{b}(\omega) = \begin{bmatrix} \widehat{\varepsilon}(x_1,\omega) \\ \widehat{\varepsilon}(x_2,\omega) \end{bmatrix}, \tag{5}$$

and the coefficient matrix

$$\mathbf{A}(\omega) = \begin{bmatrix} e^{-i\xi(\omega)(x_1-x_0)} & e^{i\xi(\omega)(x_1-x_0)} \\ e^{-i\xi(\omega)(x_2-x_0)} & e^{i\xi(\omega)(x_2-x_0)} \end{bmatrix}. \tag{6}$$

However, the coefficient matrix becomes singular (det $\mathbf{A}=0$) if

$$\xi(\omega) = \frac{n\pi}{x_2-x_1}. \tag{7}$$

Bussac et al. [18] propose an integration method in the complex domain to address this problem. However, the same authors have also shown that the noise in the recorded strain gage signals may still lead to erroneous solutions for $\mathbf{x}(\omega)$. In order to improve the solution of Eq. (3) under the presence of measurement noise, it is useful to introduce redundant measurements including force, velocity or displacement measurements. From Eq. (1), the Fourier transform of force, velocity and displacement can be expressed as

$$\widehat{F}(x,\omega) = E^*(\omega)A\left[\widehat{\varepsilon}_R(\omega)e^{-i\xi(\omega)(x-x_0)} + \widehat{\varepsilon}_L(\omega)e^{i\xi(\omega)(x-x_0)}\right], \tag{8}$$

$$\widehat{u}(x,\omega) = c^*(\omega)\left[-\widehat{\varepsilon}_R(\omega)e^{-i\xi(\omega)(x-x_0)} + \widehat{\varepsilon}_L(\omega)e^{i\xi(\omega)(x-x_0)}\right], \tag{9}$$

$$\widehat{u}(x,\omega) = l^*(\omega)\left[\widehat{\varepsilon}_R(\omega)e^{-i\xi(\omega)(x-x_0)} - \widehat{\varepsilon}_L(\omega)e^{i\xi(\omega)(x-x_0)}\right], \tag{10}$$

where

$$E^*(\omega) = \rho\left[\frac{\omega}{\xi(\omega)}\right]^2, c^*(\omega) = \frac{\omega}{\xi(\omega)} \text{ and } l^*(\omega) = \frac{i}{\xi(\omega)}. \tag{11}$$

In the present work, we perform only strain and displacement measurements. Formally, we write

$$\mathbf{b}(\omega) = \begin{bmatrix} \widehat{\varepsilon}(x_1,\omega) \\ \vdots \\ \widehat{\varepsilon}(x_Q,\omega) \\ \widehat{u}(x_{Q+1},\omega) \\ \vdots \\ \widehat{u}(x_{Q+R},\omega) \end{bmatrix} \tag{12}$$

where the subscripts Q and R represent the number of measurements for strains and displacements, respectively, at the locations x_i ($i=1,\ldots,Q+R$) on the bar. The corresponding matrix $\mathbf{A}$ reads

$$\mathbf{A}(\omega) = \begin{bmatrix} e^{-i\xi(\omega)(x_1-x_0)} & e^{i\xi(\omega)(x_1-x_0)} \\ \vdots & \vdots \\ e^{-i\xi(\omega)(x_Q-x_0)} & e^{i\xi(\omega)(x_Q-x_0)} \\ l^*(\omega)e^{i\xi(\omega)(x_{Q+1}-x_0)} & -l^*(\omega)e^{i\xi(\omega)(x_{Q+1}-x_0)} \\ \vdots & \vdots \\ l^*(\omega)e^{i\xi(\omega)(x_{Q+R}-x_0)} & -l^*(\omega)e^{i\xi(\omega)(x_{Q+R}-x_0)} \end{bmatrix}. \tag{13}$$

For redundant measurements, the equation $\mathbf{b}=\mathbf{A}\mathbf{x}$ for the unknown $\mathbf{x}$ is over-determined and cannot be solved exactly. Instead, an approximate solution is calculated by using the least squares method to minimize the scalar error $e = \|\mathbf{b}-\mathbf{A}\mathbf{x}\|^2 = (\mathbf{b}-\mathbf{A}\mathbf{x})^H(\mathbf{b}-\mathbf{A}\mathbf{x})$. Thus, the approximate solution $\mathbf{x}$ minimizing the error must satisfy the equation $\mathbf{A}^H\mathbf{b}=\mathbf{A}^H\mathbf{A}\mathbf{x}$. As long as the columns of $\mathbf{A}$ are linearly independent, the matrix $\mathbf{A}^H\mathbf{A}$ is positive definite (e.g. Strang [38]) and the unknown $\mathbf{x}$ can be determined as

$$\mathbf{x} = \left[\mathbf{A}^H\mathbf{A}\right]^{-1}\mathbf{A}^H\mathbf{b}, \tag{14}$$

where the Hermitian $\mathbf{A}^H$ (complex conjugate and transpose of $\mathbf{A}$) corresponds to the transpose of $\mathbf{A}$ if $\mathbf{A}$ is real (e.g. Magnus and Neudecker [39]). Note that a least squares solution of similar form has been presented by Hillström et al. [40] in the context of complex modulus identification based on redundant strain measurements.

In order to rule out the linear dependence of the columns of $\mathbf{A}$, we modify the propagation coefficient $\xi(\omega)$ artificially. In other words, when calculating $\mathbf{A}$, $\xi(\omega)$ is substituted by the modified propagation coefficient $\tilde{\xi}(\omega)$,

$$\tilde{\xi}(\omega) = \xi(\omega) + i\overline{\eta}\frac{d\xi(\omega)}{d\omega} \tag{15}$$

where $\overline{\eta}$ is a very small, but otherwise arbitrary, negative number; throughout our analysis, we used $\overline{\eta} = -10^{-7}$. The modified propagation coefficient $\tilde{\xi}(\omega)$ corresponds to the linear perturbation of the propagation coefficient $\xi(\omega)$ in the complex frequency domain.

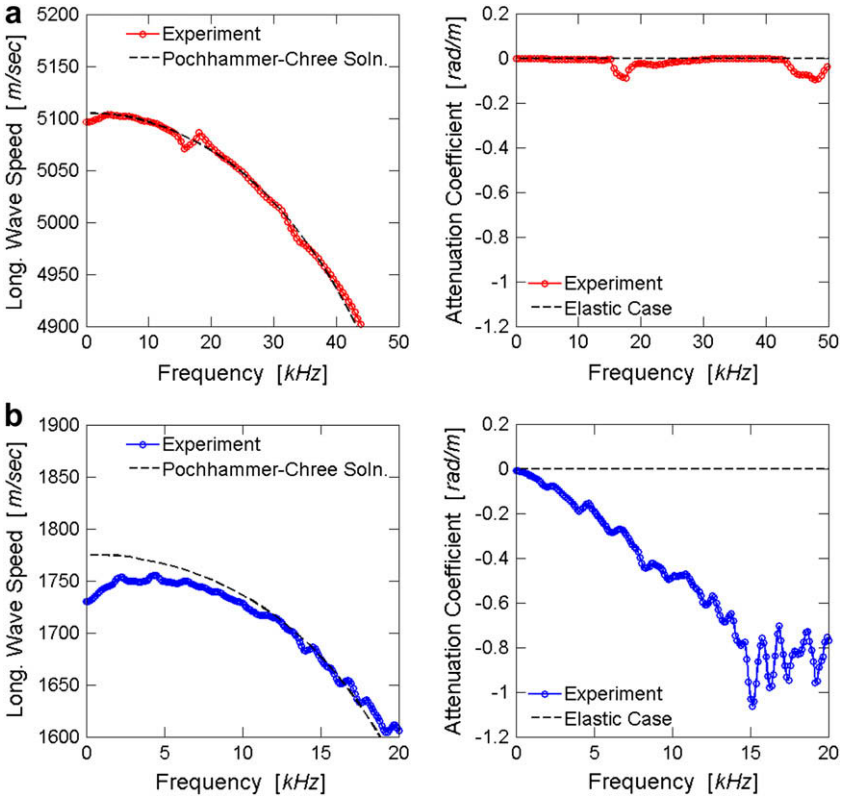

Fig. 4. (a) Propagation coefficient of aluminum bar, (left) longitudinal wave speed, and (right) attenuation coefficient, (b) Propagation coefficient of nylon bar, (left) longitudinal wave speed, and (right) attenuation coefficient.

As a result, the propagation coefficient is always complex-valued, and thus the singularity condition Eq. (7) can no longer be satisfied. Note that $\overline{\eta}$ introduces a very small artificial attenuation,

$$\tilde{\xi}(\omega) = \left[\kappa(\omega) - \overline{\eta}\frac{d\,\overline{\alpha}(\omega)}{d\omega}\right] + i\left[\overline{\alpha}(\omega) + \overline{\eta}\frac{d\kappa(\omega)}{d\omega}\right]. \tag{16}$$

As a result, even purely elastic materials ($\overline{\alpha}(\omega) = 0$) exhibit some artificial attenuation (i.e. non-zero imaginary value) which ensures the causality of the waves propagating in a bar (e.g. Bacon [14]).

In the present study we make use of a modified SHPB system with nylon input and output bars. Table 2 summarizes the technical specifications of the testing system. Each bar is equipped with three strain gages and a high contrast grid for optical displacement measurements (Model 100H, Zimmer, Germany). After using Eq. (14) to determine the leftward and the rightward traveling waves $\varepsilon_L^{\text{in}}(x_0^{\text{in}}, t)$ and $\varepsilon_R^{\text{in}}(x_0^{\text{in}}, t)$, the displacement $u_{\text{in}}(t)$ and the force $F_{\text{in}}(t)$ at the input bar/specimen interface are:

$$\widehat{u}_{\text{in}}(\omega) = l^*(\omega)\left[\widehat{\varepsilon}_R^{\text{in}}\left(x_0^{\text{in}}, \omega\right)e^{i\tilde{\xi}(\omega)x_0^{\text{in}}} - \widehat{\varepsilon}_L^{\text{in}}\left(x_0^{\text{in}}, \omega\right)e^{-i\tilde{\xi}(\omega)x_0^{\text{in}}}\right] \tag{17}$$

$$\widehat{F}_{\text{in}}(\omega) = E^*(\omega)A\left[\widehat{\varepsilon}_R^{\text{in}}\left(x_0^{\text{in}}, \omega\right)e^{i\tilde{\xi}(\omega)x_0^{\text{in}}} + \widehat{\varepsilon}_L^{\text{in}}\left(x_0^{\text{in}}, \omega\right)e^{-i\tilde{\xi}(\omega)x_0^{\text{in}}}\right] \tag{18}$$

Analogously, the displacement $\widehat{u}_{\text{out}}(\omega)$ and the corresponding force $\widehat{F}_{\text{out}}(\omega)$ at the output bar/specimen interface are determined from the output bar measurements.

2.4. Determination of the stress–strain curve

The time histories of the displacements and forces at the specimen boundaries, $u_{\text{in}}(t)$, $u_{\text{out}}(t)$, $F_{\text{in}}(t)$ and $F_{\text{out}}(t)$ are obtained from applying the inverse Fourier transform $f(t) = \frac{1}{2\pi}\int_{-\infty}^{\infty}\widehat{f}(\omega)e^{i\omega t}\mathrm{d}t$ to $\widehat{u}_{\text{in}}(\omega)$, $\widehat{u}_{\text{out}}(\omega)$, $\widehat{F}_{\text{in}}(\omega)$ and $\widehat{F}_{\text{out}}(\omega)$, respectively. The input force $F_{\text{in}}(t)$ is considered as a redundant measurement; it is used to verify the condition of quasi-static equilibrium of a dynamically loaded specimen,

$$F_{\text{out}}(t) - F_{\text{in}}(t) \cong 0. \tag{19}$$

The spatial average of the logarithmic axial strain $\varepsilon(t)$ within the specimen reads

$$\varepsilon(t) = \ln\left(1 + \frac{u_{\text{out}}(t) - u_{\text{in}}(t)}{L_0}\right) \tag{20}$$

where L_0 denotes the initial length of the specimen. Using the output force measurement, we calculate the true stress

$$\sigma(t) = \frac{F_{\text{out}}(t)}{A_0}\exp[2\nu\varepsilon(t)], \tag{21}$$

where A_0 is the initial cross-sectional area and ν is the elastic Poisson's ratio. In the present work, it is assumed that the Poisson's ratio is constant, i.e. it depends neither on the strain nor on the strain rate. The final true stress–strain curve is then found from the combination of the stress and strain history functions,

$$\sigma(\varepsilon) = \sigma(t)\varepsilon(t). \tag{22}$$

3. Experimental results

All experiments are performed on polyurea. This rubber-like material has a mass density of 1.0 g/cm^3 and an elastic modulus of about 100 MPa.

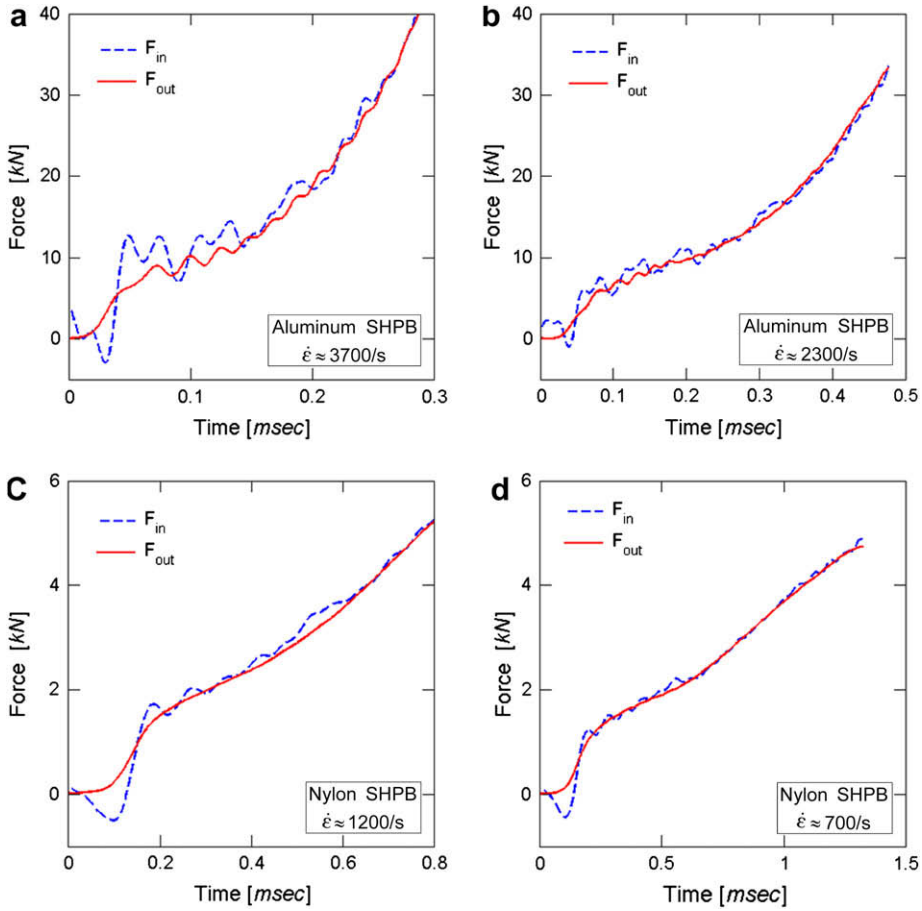

Fig. 5. Comparison of forces between input bar and output bar from SHPB tests from aluminum bar tests: (a) $\dot{\varepsilon} \approx 3700/s$, (b) $\dot{\varepsilon} \approx 2300/s$ and nylon bar tests: (c) $\dot{\varepsilon} \approx 1200/s$, (d) $\dot{\varepsilon} \approx 700/s$.

3.1. Experiments using the universal testing machine

Representative stress–strain curves for true strain rates of up to 10/s are determined from experiments on the universal testing machine using cylindrical specimens of diameter $D_0 = 10$ mm and length $L_0 = 10$ mm. All experiments are carried out under displacement control up to a maximum true compressive strain of 100% (which corresponds to an engineering compressive strain of 63%). In order to achieve a constant true strain rate $\dot{\varepsilon}_0$, a velocity profile $\dot{u}_{\text{in}}(t)$ of exponential shape is applied to the top of the specimen,

$$\dot{u}_{\text{in}}(t) = -L_0 \dot{\varepsilon}_0 \exp(\dot{\varepsilon}_0 t). \tag{23}$$

The Poisson's ratio is determined from the experiments performed at true compressive strain rates of up to 1/s. Based on the DIC measurements of the specimen diameter $D = D(t)$, we calculate the logarithmic radial strain ε_r,

$$\varepsilon_r = \ln\left(\frac{D}{D_0}\right), \tag{24}$$

where D_0 denotes the initial specimen diameter. The experimental data depicted in Fig. 2 shows the linear relationship between the logarithmic radial strain and the logarithmic axial strain. Upon evaluation of the slope, we find a Poisson's ratio of $\nu = 0.448$.

The data acquisition rate of the DIC system is limited to about 7 Hz. Thus, we only use the DIC system for the slowest experiments and make use of the actuator position measurement (LVDT) to determine the effective axial displacement at higher strain rates. The comparison of the LVDT readout with the DIC measurement yields an overall stiffness of the testing frame of about 100 kN/mm. The measured true stress–strain curves are shown in Fig. 3a for true strain rates of about 10^{-2}/s, 10^{-1}/s, 10^{0}/s, and 10^{1}/s. The corresponding true strain rate versus true strain curves are depicted in Fig. 3b. For the slowest experiment ($\dot{\varepsilon}_0 \cong 10^{-2}/s$), the slope of the stress–strain curve (Fig. 3a) decreases significantly at a stress of about 0.1; subsequently, the stress–strain curve changes its shape from concave to convex at an axial strain of about 0.3. Due to the characteristic rubber chain locking behavior, the stress level increases monotonically throughout the entire experiment from 6 MPa at $\varepsilon = 0.1$ to 13.5 MPa at $\varepsilon = 1.0$. For the next higher strain rate ($\dot{\varepsilon}_0 \cong 10^{-1}/s$), the overall stress level is about 12% higher. Similarly, the shape of the stress–strain curve is preserved for strain rates of 10^{0}/s and 10^{1}/s, but the stress level increases by 35% and 61%, respectively, compared to that at 10^{-2}/s.

3.2. Experiments using conventional SHPB systems

Appendix A outlines the identification of the frequency-dependant coefficients $c(\omega)$ and $\overline{\alpha}(\omega)$ for both the aluminum and nylon bars. The results are presented in Fig. 4 together with the Pochhammer-Chree solution (e.g. Graff [41]). These experimentally obtained coefficients are used throughout our analysis of the waves in both the conventional and the modified SHPB systems.

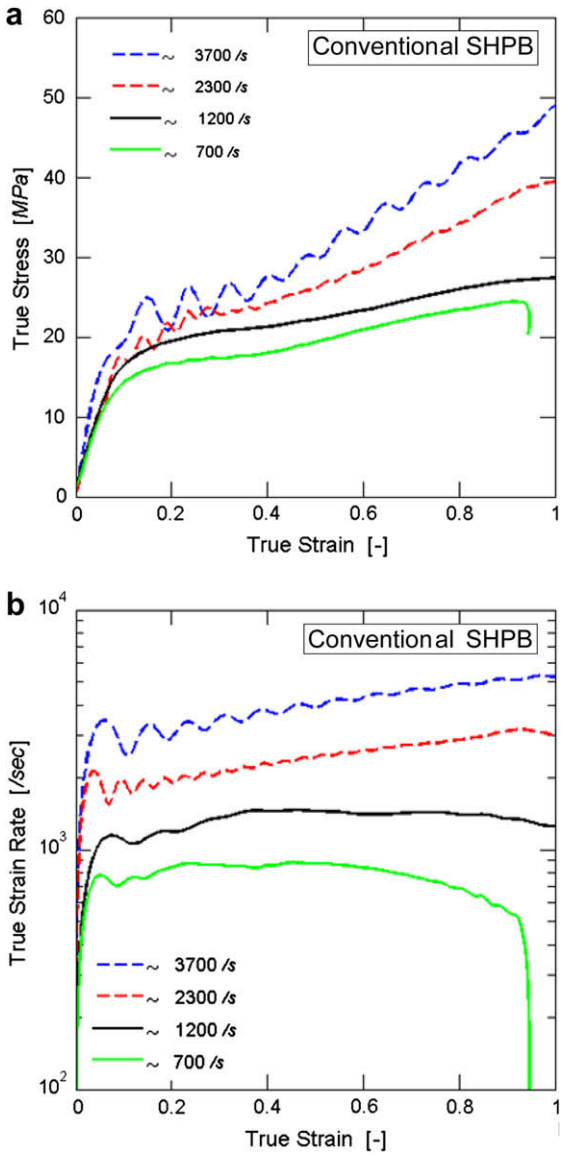

Fig. 6. Test results from the SHPB systems: (a) True stress–strain curves, (b) True strain rate versus true strain curves.

3.2.1. Aluminum bar system

Experiments at high strain rates are performed on the conventional aluminum SHPB system. Cylindrical polyurea specimens with $D_0 = 20$ mm and $L_0 = 5$ mm are used on the aluminum system. Average strain rates of $\dot{\varepsilon} = 3700/s$ and $\dot{\varepsilon} = 2300/s$ are achieved at striker velocities of 13 m/s and 9 m/s, respectively. To verify the quasi-static equilibrium throughout the experiments, both the input and output force are depicted in Fig. 5a and b. The poor agreement of the force measurements for 3700/s may be read as lack of equilibrium (e.g. Aloui et al. [42]). However, for the present experiments, this observation is attributed to the low signal-to-noise ratio for the input force measurements. Due to the pronounced mismatch between the force amplitude of the incident wave ($F_{inc} = A_{AL}\rho_{AL}c_{AL}V_{str}/2 \approx 120$ kN for 13 m/s) and the specimen resistance (e.g. $F_{\text{in}} = A_{spc}\sigma_{spc} \approx 15kN$ at $\varepsilon = 0.5$), most of the incident wave is reflected at the input bar/specimen interface which ultimately results in a poor input force measurement (see e.g. Grolleau et al. [43] for details on the force measurement accuracy). The incident wave exhibits some Pochhammer-Chree oscillations due to the lateral inertia of the 40 mm diameter aluminum bars. Consequently, we observe some non-monotonic behavior in the stress–strain curves for 3700/s and 2300/s in Fig. 6a. The overall shape of the curve is very similar to that for static loading, but the stress level is almost three to four times higher.

3.2.2. Nylon bar system

Another set of high strain rate experiments (1200/s and700/s) are performed using smaller diameter specimens ($D_0 = 10$ mm, $L_0 = 5$ mm) on the nylon bar SHPB system. Recall that the main reason for changing from aluminum to nylon bars is to increase the maximum duration of the experiments from $T_{\text{exp}} = 472$ μs to 1255 μs. At the same time, the use of nylon significantly reduces the impedance mismatch between the bars and the polyurea specimen. This improves the force measurement accuracy, notably, that of the input force. Striker velocities of 8 m/s and 6 m/s are needed to obtain an average strain rate of $\dot{\varepsilon} \cong 1200/s$ and $\dot{\varepsilon} \cong 700/s$, respectively. Higher striker velocities would cause inelastic deformation in the bars upon striker impact. On the other hand, for a maximum loading duration of 1255 μs, lower striker velocities would not achieve the desired maximum true compressive strain of $\varepsilon = 1.0$.

There are less signal oscillations in the nylon than in the aluminum system because of its higher signal-to-noise ratio. Furthermore, due to the lower striker velocities and the wave attenuation in the nylon input bar, there are less severe Pochhammer-Chree oscillations in the incident wave signal as compared to the aluminum system (see Fig. 5). Therefore, relatively smooth stress–strain curves are obtained from the dynamic experiments onthe nylon bar system (Fig. 6a). The exact evolution of the true strain rates as a function of the true strain are shown in Fig. 6b. Unlike for the experiments on the aluminum bar system, the true strain rate is no longer increasing in a monotonic manner. This isdue to the lower amplitude of the incident force (e.g. $F_{inc} = A_{NY}\rho_{NY}c_{NY}V_{str}/2 \cong 7.6$ kN for $\dot{\varepsilon} = 700/s$) which is now of the same order of magnitude as the specimen resistance ($F_{\text{in}} = A_{spc}\sigma_{spc} \cong 2.5kN$). Thus, as the specimen resistance increases throughout the experiment, the magnitude of the reflected wave decreases; as a result, despite the logarithmic strain definition, the engineering strain rate no longer increases due to the decreasing interface velocity.

3.3. Experiments using the modified SHPB system

Experiments are performed on the modified nylon SHPB system using the hydraulic actuator in an open mode, which is different from the conventional closed loop mode of servo-hydraulic testing machines. In this open loop mode, the user can preset the position of the inlet servo valve. Furthermore, the initial pressure of the inflowing fluid may be controlled. However, the user has no active control of the actuator velocity throughout the experiment. Actuator piston velocities of up to 5 m/s may be achieved in this mode of operation. Here, we perform experiments at 4 m/s, 1 m/s, 0.5 m/s, and 0.1 m/s which resulted in average compressive strain rates of about 1000/s, 110/s, 36/s and 10/s.

Three strain gages and one displacement measurement are taken into account (per bar) to reconstruct the waves in either bar using the above deconvolution technique.[1] The comparison of the measured input and output force histories confirms the quasi-static

[1] The only exception is the input bar in the experiment at 110/s where one of the three strain gauge signals was not properly recorded. Therefore, only two strain gages and one displacement measurement were taken into account for that experiment.

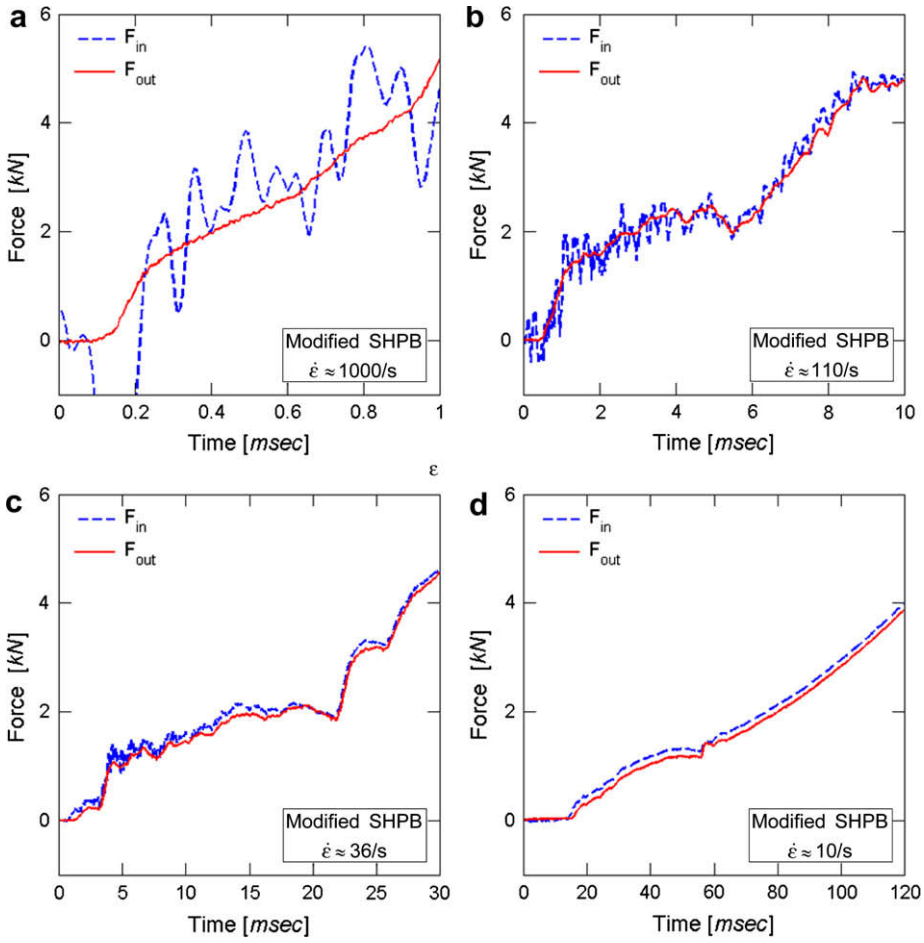

Fig. 7. Comparison of forces between input bar and output bar from the modified SHPB tests: (a)$\dot{\varepsilon} \approx 1000/s$, (b)$\dot{\varepsilon} \approx 110/s$, (c)$\dot{\varepsilon} \approx 36/s$, (d)$\dot{\varepsilon} \approx 10/s$.

equilibrium for 110/s, 36/s and 10/s (Fig. 7). The differences between the input and output force for 1000/s are associated with the poor quality of the deconvolution based estimate of the input force; the accuracy of the optical displacement measurement system decreases substantially at high loading velocities leading to severe oscillations in the input force history. However, considering that the higher velocity cases (Fig. 5) show the good force agreement, the quasi-static equilibrium can also be assumed for the strain rate of 1000/s. A significant force drop is found at $t \approx 5$ ms, 20 ms, and 60 ms for the strain rates of 110/s, 36/s and 10/s, respectively. This force drop is due to the premature partial failure of the fixed end support of the output bar that causes a short unloading-reloading cycle. The same force drops are also found in the stress versus strain curve (Fig. 8a) at strains of 55%, 60%, and 25% for strain rates of 110/s, 36/s and 10/s, respectively.

3.4. Comment on the signal oscillations

There are two characteristic time scales associated with the experiments on the modified SHPB system. The short time scale corresponds to the round trip time of an elastic wave traveling through the specimen, $\Delta t_s \cong 11$ μs. The second time scale is much longer; it is associated with the round trip of an elastic wave traveling through the input bar, $\Delta t_{\text{in}} \cong 3600$ μs. The experiment at an average strain rate of 1000/s remains unaffected by the large time scale as the total duration of the experiment (≈ 1000 μs) is still shorter than Δt_{in}. However, already at a strain rate of 110/s, the duration of the experiment ($\Delta t_{\text{exp}} \approx 10^4$ μs) exceeds Δt_{in}. As a result, the shape and amplitude of the incident wave is not only determined by the velocity of the hydraulic actuator, but also by the leftward traveling wave that has been reflected by the specimen. Consequently, the incident wave changes with a periodicity of Δt_{in}. In the present experiments, the first reflected wave is a tensile wave which reduces the initial magnitude of the compressive incident wave. Hence, the rate of loading decreases before the rate of loading increases again after the next period of Δt_{in}. Therefore, this abrupt change of the loading rate has a periodicity of Δt_{in}. The corresponding strain rate versus strain curve shows a pronounced decrease in strain rate; since the strain increases only little during a period of reduced loading rate, we observe sharp drops in the strain rate versus total strain curve. For lower average strain rates, this number of strain rate drops increases further. Formally, we may write

$$n \cong \frac{\varepsilon_{tot} / |\dot{\varepsilon}_{ave}|}{\Delta t_{\text{in}}}, \tag{25}$$

where n is the number of the expected drops in strain rate associated with the wave reflections in the input bar. This number is 2, 7, and 27 for the experiments at average strain rates of 110/s, 36/s and 10/s. In the limiting case of static loading, we have $n \to \infty$ which ultimately results in a constant strain rate versus strain curve. In addition to loading velocity changes associated with wave reflections in the input bar, our experimental results are also affected by other sources of vibrations. These include wave reflections within

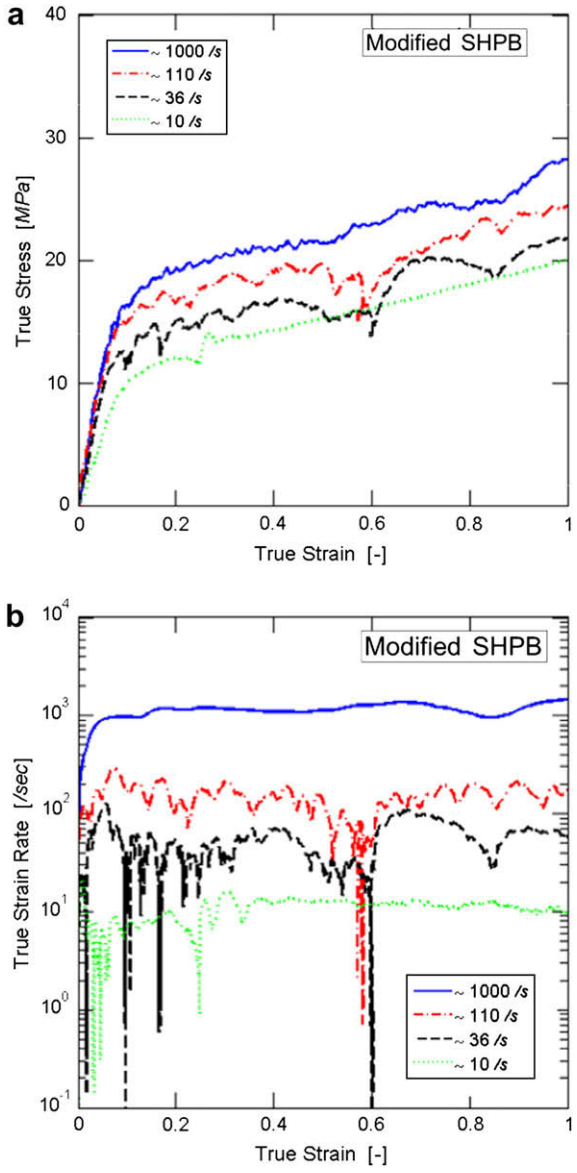

Fig. 8. Test results from the modified SHPB system: (a) True stress–strain curves, (b) True strain rate versus true strain curves.

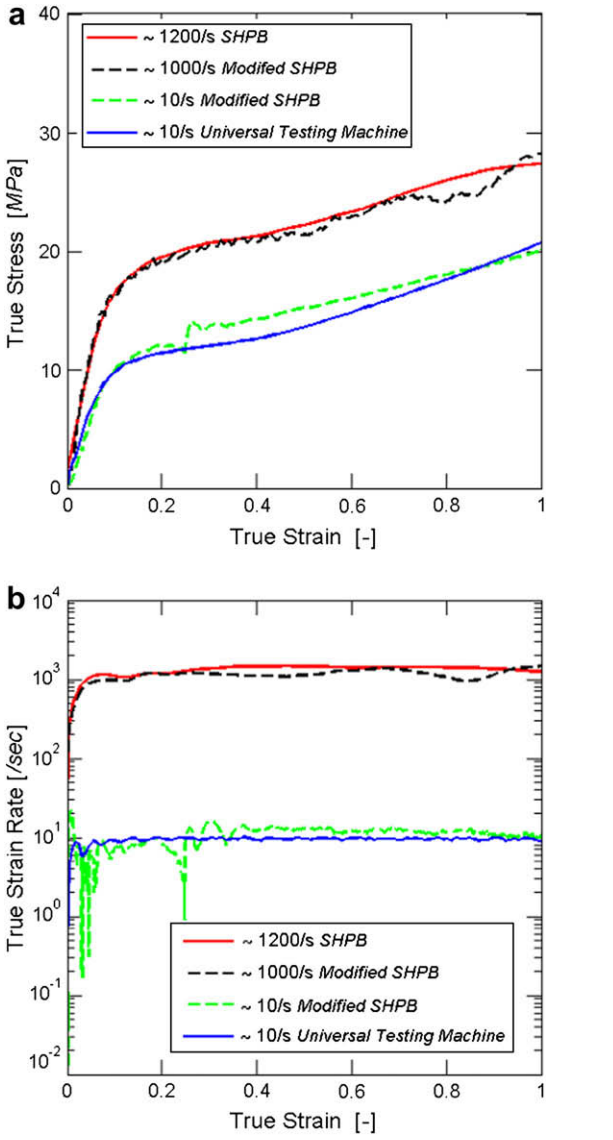

Fig. 9. Comparison of the results from the modified SHPB with those from other two testing methods: (a) True stress–strain curves, (b) True strain rate versus true strain curves (For interpretation of the references to colour in this figure, the reader is referred to the web version of this article).

the output bar as well as vibrations in the fixed end support system and the hydraulic actuator. Therefore, the exact identification of all strain rate drops in Fig. 8b according to Eq. (25) has been omitted.

4. Discussion

4.1. Experimental results

To validate our experimental data, we first checked the consistency among the results obtained from different testing methods. Fig. 9 shows selected stress–strain curves obtained from the modified SHPB system (dashed lines) next to the results from the conventional SHPB (red solid line) and the universal testing machine (blue solid line). For 1000/s, the modified SHPB result shows reasonably good agreement with the conventional SHPB curve for 1200/s. Analogously, for the average strain rate of 10/s, the stress–strain curve obtained from the modified SHPB test corresponds well to that obtained from the test on the universal testing machine. Recall that the perturbation of the stress–strain curve for the modified SHPB system at about 25% strain is due to the partial premature failure of the output bar end support system. The stress level from the modified SHPB is slightly higher after partial support failure which is attributed to differences in the strain rate.

The data in Fig. 10a show the stress as a function of the strain rate for different levels of strain: 10%, 50% and 90%. The effect of strain rate is more pronounced at large strains. For instance, at a strain of 0.1, the stress level increases by 317% when increasing the strain rate from $\dot{\varepsilon} = 10^{-2}/\mathrm{s}$ to $\dot{\varepsilon} = 3700/\mathrm{s}$(increase from 6 kN to 19 kN); at a strain of 0.9, the stress level increases by 360% over the same range of strain rates (from 12.5 kN at $\dot{\varepsilon} = 10^{-2}/\mathrm{s}$ to 45 kN at $\dot{\varepsilon} = 3700/\mathrm{s}$). In the same figure, the non-linear empirical function,

$$\sigma = A\left(\frac{\dot{\varepsilon}}{\dot{\varepsilon}_0}\right)^B + C \tag{26}$$

has been fitted to the experimental data using a reference strain rate of $\dot{\varepsilon}_0 = 10^{-2}/\mathrm{s}$. A[MPa] represents the amplitude of the curve,

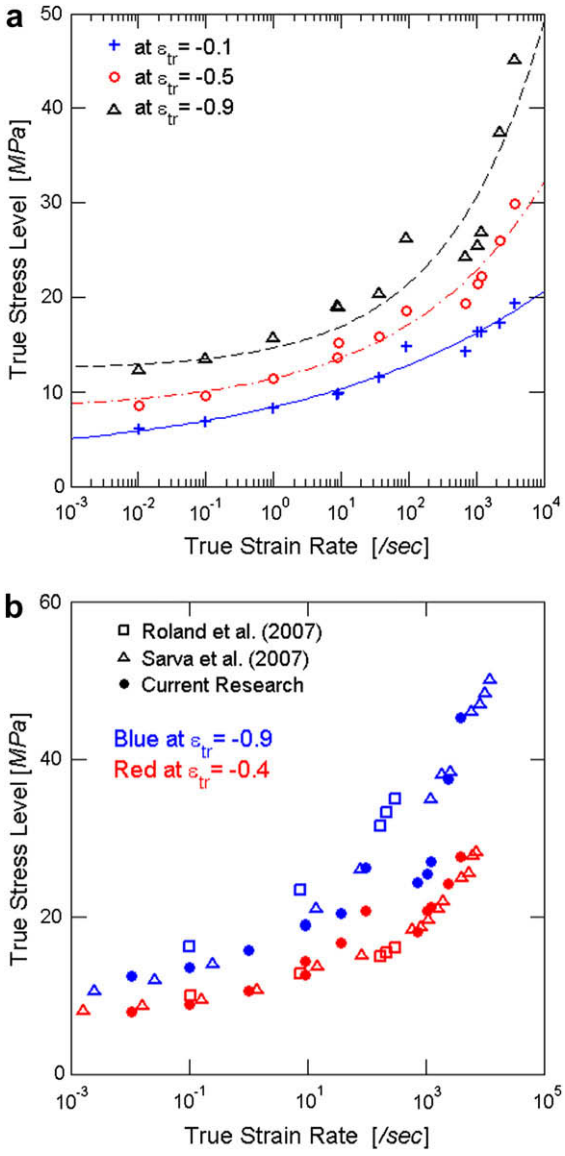

Fig. 10. True stress as a function of the strain rate at selected strain levels: (a) fit of Eq. (26) to the results from the present study. (b) Comparison of the results with previous studies.

$B[-]$ represents the sensitivity of the strain rate, and C[MPa] represents the asymptotic stress level for infinitely slow loading conditions. The values of these parameters are given in Table 3.

4.2. Intermediate strain rate testing systems

The present experimental study confirms the high strain rate sensitivity of the polyurea material which has been reported in earlier studies. Roland et al. [9] performed a series of tensile tests using a custom-made pulley system in a drop tower to perform uniaxial tensile tests at intermediate and high strain rates. Sarva et al. [37] used an enhanced universal testing machine to perform compression experiments at strain rates of up to 80/s while an aluminum SHPB system with a striker bar length of 3 m has been used to perform experiments at strain rates above 800/s. The comparison of the present experimental data with the results of Sarva et al. [37] and Roland et al. [9] confirms the validity of the measurements with the modified SHPB system (Fig. 10b).

Table 3
Calibrated coefficients describing the strain rate effect on the deformation resistance of polyurea at three different strain levels. The reference strain rate in Eq. (26) is $\dot{\varepsilon}_0 = 10^{-2}/$, which corresponds to the lowest strain rate in the present experiments.

	A[MPa]	$B[-]$	C[MPa]
at $\varepsilon = -0.1$	3.46	0.120	2.37
at $\varepsilon = -0.5$	1.25	0.215	8.05
at $\varepsilon = -0.9$	0.561	0.303	12.4

The implementation of the deconvolution technique by Bussac et al. [18] leads to a stable algorithm that is convenient to use for the reconstruction of dispersive waves in bars based on redundant measurements. Thus, the theoretical limitation of the duration of experiments on SHPB systems is successfully overcome. In combination with a hydraulic actuator, the entire range of low to high strain rates could be covered using a single testing system. The comparison with conventional SHPB experiments at high strain rates and universal testing machine experiments at low strain rates has confirmed the validity of the modified SHPB technique. However, there are still two difficulties associated with our modified SHPB system which need to be addressed in the future:

1) Displacement and/or velocity measurement accuracy: the accuracy of the deconvolution technique relies heavily on accurate displacement measurements (in particular at low strain rates). The present optical technique provided good results for loading velocities of up to 0.5 m/s, but significant errors became visible at larger loading velocities.
2) Quality of the loading pulse at specimen interfaces. In order to achieve approximately constant strain rates, the ideal loading pulse should be such that the bar/specimen interfaces move at constant velocities.

The first difficulty may be resolved through the use of improved measurement equipment. Alternatively, the deconvolution technique for high loading velocities may also be applied using strain gage measurements only. However, it is very challenging to overcome the second difficulty. As an intermediate strain rate experiment takes much longer than a wave round trip in the input bar, the input bar/specimen interface velocity is not constant even if the hydraulic piston moves at a constant velocity. Simple wave analysis shows that a period of high velocity loading is followed by a period of loading at a lower rate; the length of each period corresponds to the round trip time for a wave traveling in the input bar. The same holds true for the output bar/specimen interface velocity which is affected by the round trip time in the output bar. Consequently, the strain rate in our intermediate strain rate experiments was not constant.

For the desired maximum true compressive strain of $\varepsilon = 1.0$, the total duration of an intermediate strain experiment at 50/s is $T_{exp} = 20$ ms – irrespective of the specimen geometry. Conceptually, there exist several solutions to this problem:

(1) Conventional nylon SHPB system with a striker bar length of $1740 \times 0.02 \times 0.5 = 17.4$ m along with a 35 m long input bar and a 17.5 m long output bar. In this configuration, all strain gages can be positioned such that the rightward and leftward traveling waves do not superpose at the strain gage locations.
(2) Conventional nylon SHPB system with a 17.5 m long striker bar and 17.5 m long input and output bars. In this case, a deconvolution method needs to be used to reconstruct the waves in the input and output bars. However, the input bar is still sufficiently long to guarantee that the round trip time is greater than the duration of the experiment.

(3) Hydraulic nylon SHPB system with 17.5 m long input and output bars. Based on the assumption that the hydraulic piston moves at a constant velocity, this system will provide the same capabilities as the previous system.

As an alternative to very long input and output bars, one may chose the opposite strategy. Note that the magnitude of the oscillations is proportional to the change in force level in the specimen over the time Δt_{in}. Thus, the shorter the input bar, the smaller the oscillation magnitude. One could therefore envision very short (e.g. <0.5 m) small diameter input and output bars. In this case, we have $\Delta t_{\text{in}} = 0.57$ ms and hence $\Delta t << T_{\text{exp}}$

However, since the modified SHPB system requires two displacement measurement sensors (notably for low strain rate experiments), one can also use these sensors to measure directly the displacements of the respective bar/specimen interfaces. Hence the strain history can be measured without using the deconvolution algorithm. The bars would therefore only serve as load cell to measure the force history. Unless the quasi-static equilibrium needs to be verified experimentally, a single force measurement is satisfactory. Moreover, it may be worth considering a piezo-electric sensor to measure the force, thereby completely eliminating the use of bars to perform the experiments at low, intermediate and high strain rates. As our hydraulic piston cannot provide a constant loading velocity above 0.5 m/s, a striker bar may also be used to load the specimen. The only unknown which is left in this system is the realization of the "fixed" boundary condition. Further research needs to be carried out to design a support point that does not introduce spurious oscillation into the testing system.

5. Conclusion

The modified SHPB system of Zhao and Gary [13] has been used to perform compression tests on polyurea at low, intermediate and high strain rates. It is composed of nylon input and output bars, while the striker bar is substituted by a hydraulic actuator. Using the deconvolution technique by Bussac et al. [18], the time limitation of conventional SHPB systems may be overcome, thereby enabling the use of the modified SHPB system for low and intermediate strain rate experiments of long duration. The experiments confirm the known strain rate sensitivity of polyurea. The measured stress levels correspond well to earlier results which have been obtained from tests on conventional SHPB systems with very long bars. Although the intrinsic time limitation of SHPB systems could be overcome, this study also shows that it is still not possible to perform experiments at reasonably constant strain rates with this technique. This is due to the finite length of the input and output bars which causes a periodic change in loading velocity. It is shown that intermediate strain rate SHPB experiments require either very long bars (>20 m) or very short bars (<0.5 m) in order to achieve an approximately constant strain rate throughout the entire experiment.

Acknowledgement

The authors are grateful to Professor Gerard Gary and Mr. Vincent de Greef from École Polytechnique for sharing their know-how on SHPB experiments. Mr. Raymond Barre and Mr. Erik Guimbretiere are thanked for their technical assistance. Professor Tomasz Wierzbicki from MIT is thanked for valuable discussion. Thanks are also due to Mr. Carey Walters and Mr. Fabien Ebnoether for their help on performing the low strain rate experiments. The partial financial support through Office of Naval Research (ONR) Grant #N00014-07-1-0821 and the French National Center for Scientific Research (CNRS) is gratefully acknowledged.

Appendix A. Identification of the wave propagation coefficient for viscoelastic bars

The complex-valued propagation coefficient $\xi(\omega)$ is a function of both the geometric and material properties of the bars. If the complex modulus of the viscoelastic bar material is known, $\xi(\omega)$ may be calculated from solving Pochhammer-Chree's frequency equation (Zhao and Gary [44]). As an alternative, we make use of an experimental method that considers both geometric dispersion and viscous attenuation within the framework of the 1-D wave theory (e.g. Bacon [45], Lundberg and Blanc [46]) to determine $\xi(\omega)$. Recall the solution of the one-dimensional wave equation for viscoelastic bars,

$$\widehat{\varepsilon}(x,\omega) = \widehat{\varepsilon}_R(\omega)e^{-i\xi(\omega)x} + \widehat{\varepsilon}_L(\omega)e^{i\xi(\omega)x} \tag{A-1}$$

where $\widehat{\varepsilon}_R(\omega)$ and $\widehat{\varepsilon}_L(\omega)$ are the rightward and the leftward traveling strain waves, and $\xi(\omega)$ is the propagation coefficient of the bars,

$$\xi(\omega) = \kappa(\omega) + i\overline{\alpha}(\omega) = \frac{\omega}{c(\omega)} + i\overline{\alpha}(\omega). \tag{A-2}$$

$\kappa(\omega)$ is the wave number, $c(\omega)$ is the frequency-dependant longitudinal wave propagation speed, and $\overline{\alpha}(\omega) \le 0$ represents the attenuation coefficient. Note that $c(\omega)$ and $\overline{\alpha}(\omega)$ are even functions of ω while $\kappa(\omega)$ is an odd function in the frequency space.

After performing an impact test on a single bar, the transfer function

$$H(\omega) = -\frac{\widehat{\varepsilon}_{ref}(\omega)}{\widehat{\varepsilon}_{inc}(\omega)} = e^{-2i\xi(\omega)d}, \tag{A-3}$$

is determined from the measured incident and reflected strain histories $\widehat{\varepsilon}_{inc}(\omega)$ and $\widehat{\varepsilon}_{ref}(\omega)$, respectively; d is the distance between the strain gage location and the free end of the bar. From the above equation, two components of the propagation coefficient can be identified using the relations

$$\kappa(\omega) = -\frac{\arg[H(\omega)]}{2d} \text{ and } \overline{\alpha}(\omega) = \frac{\ln[|H(\omega)|]}{2d}. \tag{A-4}$$

References

[1] McGrum NG, Buckley CP, Bucknal CB. Principles of polymer engineering. New York, NY: Oxford University Press; 1997. p. 117.
[2] Yi J, Boyce MC, Lee GF, Balizer E. Large deformation rate-dependent stress–strain behavior of polyurea and polyurethanes. Polymer 2006;47:319–29.
[3] Song B, Chen W, Lu WY. Mechanical characterization at intermediate strain rates for rate effects on an epoxy syntactic foam. International Journal of Mechanical Sciences 2007;49:1336–43.
[4] Gray GT, Blumenthal WR. Split-Hopkinson pressure bar testing of soft materials, ASM Handbook. Mechanical Testing and Evaluation 2000;8:488–96.
[5] Zhao H, Gary G, Klepaczko JR. On the use of a viscoelastic split Hopkinson pressure bar. International Journal of Impact Engineering 1997;19:319–30.
[6] Chen W, Zhang B, Forrestal MJ. A split Hopkinson bar technique for low-impedance materials. Experimental Mechanics 1999;39:81–5.
[7] Sharma A, Shukla A, Prosser RA. Mechanical characterization of soft materials using high speed photography and split Hopkinson pressure bar technique. Journal of Materials Science 2002;37:1005–17.
[8] Hoo Fatt MS, Bekar I. High-speed testing and material modeling of unfilled styrene butadiene vulcanizates at impact rates. Journal of Materials Science 2004;39:6885–99.
[9] Roland CM, Twigg JN, Vu Y, Mott PH. High strain rate mechanical behavior of polyurea. Polymer 2007;48:574–8.
[10] Lundberg B, Henchoz A. Analysis of elastic-waves from 2-point strain-measurement. Experimental Mechanics 1977;17:213–8.
[11] Yanagihara N. New measuring method of impact force. Bulletin of the Japan Society of Mechanical Engineers 1978;21:1085–8.
[12] Park SW, Zhou M. Separation of elastic waves in split Hopkinson bars using one-point strain measurements. Experimental Mechanics 1999;39:287–94.
[13] Zhao H, Gary G. A new method for the separation of waves. Application to the SHPB technique for an unlimited duration of measurement. Journal of the Mechanics and Physics of Solids 1997;45:1185–202.

[14] Bacon C. Separation of waves propagating in an elastic or viscoelastic Hopkinson pressure bar with three-dimensional effects. International Journal of Impact Engineering 1999;22:55–69.
[15] Casem DT, Fourney W, Chang P. Wave separation in viscoelastic pressure bars using single point measurements of strain and velocity. Polymer Testing 2003;22:155–64.
[16] Jacquelin E, Hamelin P. Block-bar device for energy absorption analysis. Mechanical Sytems and Signal Processing 2001;15:603–17.
[17] Jacquelin E, Hamelin P. Force recovered from three recorded strains. International Journal of Solids and Structures 2003;40:73–88.
[18] Bussac MN, Collet P, Gary G, Othman R. An optimization method for separating and rebuilding one-dimensional dispersive waves form multi-point measurements. Application to elastic or viscoelastic bars. Journal of the Mechanics and Physics of Solids 2002;50:321–49.
[19] Othman R, Gary G. Testing aluminum alloy from quasi-static to dynamic strain-rates with a modified split Hopkinson bar method. Experimental Mechanics 2007;47:295–9.
[20] Othman R, Guegan P, Challita G, Pasco F, LeBreton D. A modified servo-hydraulic machine for testing at intermediate strain rates. International Journal of Impact Engineering 2009;36:460–7.
[21] Chou SC, Roberstson KD, Rainey JH. The effect of strain rate and heat developed during deformation on the stress–strain curve of plastics. Experimental Mechanics 1973;13:422–32.
[22] Boyce MC, Parks DM, Argon AS. Large inelastic deformation of glassy polymers. Part I: rate dependent constitutive model. Mechanics of Materials 1988;7:15–33.
[23] Walley SM, Field JE, Pope PH, Safford NA. A study of the rapid deformation behaviour of a range of polymers. Philosophical Transactions of the Royal Society of London Series A-Mathematical Physical and Engineering Sciences 1989;328:1–33.
[24] Cady CM, Blumenthal WR, Gray GT, Idar DJ. Determining the constitutive response of polymeric materials as a function of temperature and strain rate. Journal de Physique IV 2003;110:27–32.
[25] Siviour CR, Walley SM, Proud WG, Field JE. The high strain rate compressive behaviour of polycarbonate and polyvinylidene difluoride. Polymer 2005;46:12546–55.
[26] Mulliken AD, Boyce MC. Mechanics of the rate-dependent elastic-plastic deformation of glassy polymers from low to high strain rates. International Journal of Solids and Structures 2006;43:1331–56.
[27] Mulliken AD, Soong SY, Boyce MC, Cohen RE. High-rate thermomechanical behavior of poly(vinyl chloride) and plasticized poly(vinyl chloride). Journal de Physique IV 2006;134:217–23.
[28] Bordonaro CM, Krempl E. The effect of strain rate on the deformation and relaxation behavior of 6/6 nylon. Polymer Engineering and Science 1992;32:1066–72.
[29] Khan AS, Farrokh B. Thermo-mechanical response of nylon 101 under uniaxial and multi-axial loadings: part I, Experimental results over wide ranges of temperatures and strain rates. International Journal of Plasticity 2006;22:1506–29.
[30] Gray GT, Blumenthal WR, Trujillo CP, Carpenter RW. Influence of temperature and strain rate on the mechanical behavior of Adiprene L-100. Journal de Physique IV 1997;7:523–8.
[31] Rao S, Shim VPW, Quah SE. Dynamic mechanical properties of polyurethane elastomers using a nonmetallic Hopkinson bar. Journal of Applied Polymer Science 1997;66:619–31.
[32] Song B, Chen W. One-dimensional dynamic compressive behavior of EPDM rubber. Journal of Engineering Materials and Technology, Transaction of the ASME 2003;125:294–301.
[33] Song B, Chen W. Dynamic compressive behavior of EPDM rubber under nearly uniaxial strain conditions. Journal of Engineering Materials and Technology, Transaction of the ASME 2004;126:213–7.
[34] Shergold OA, Fleck NA, Radford D. The uniaxial stress versus strain response of pig skin and silicon rubber at low and high strain rates. International Journal of Impact Engineering 2006;32:1384–402.
[35] Roland CM. Mechanical behavior of rubber at high strain rates. Rubber Chemistry and Technology 2006;79:429–59.
[36] Amirkhizi AV, Isaacs J, McGee J, Nemat-Nasser S. An experimentally-based viscoelastic constitutive model for polyurea, including pressure and temperature effects. Philosophical Magazine 2006;86:5847–66.
[37] Sarva SS, Deschanel S, Boyce MC, Chen W. Stress–strain behavior of a polyurea and a polyurethane from low to high strain rates. Polymer 2007;48:2208–13.
[38] Strang G. Introduction to applied mathematics. Wellesley, MA: Wellesley-Cambridge Press; 1985. p. 32.
[39] Magnus JR, Neudecker H. Matrix differential calculus with applications in statics and econometrics. Chichester, England: John Wiley & Sons Ltd.; 1988. p. 15.
[40] Hillström L, Mossberg M, Lundberg B. Identification of complex modulus from measured strains on an axially impacted bar using least squares. Journal of Sound and Vibration 2000;230:689–707.
[41] Graff KF. Wave motion in elastic solids. Mineola, NY: Dover Publications, Inc.; 1975. p. 470.
[42] Aloui S, Othman R, Poitou A, Guégan P, El-Borgi S. Non-parametric identification of the non-homogeneous stress in high strain-rate uni-axial experiments. Mechanics Research Communications 2008;35:392–7.
[43] Grolleau V, Gary G, Mohr D. Biaxial testing of sheet materials at high strain rates using viscoelastic bars. Experimental Mechanics 2008;48:293–306.
[44] Zhao H, Gary G. A three dimensional analytical solution of the longitudinal wave propagation in an infinite linear viscoelastic cylindrical bar. Application to experimental techniques. Journal of the Mechanics and Physics of Solids 1995;43:1335–48.
[45] Bacon C. An experimental method for considering dispersion and attenuation in a viscoelastic Hopkinson bar. Experimental Mechanics 1998;38:242–9.
[46] Lundberg B, Blanc RH. Determination of mechanical material properties from the two-points response of an impacted linearly viscoelastic rod specimen. Journal of Sound and Vibration 1988;126:97–108.